Electronic Supporting Information (ESI)

High and selective CO_2 capture of two mesoporous acylamide-functionalized *rht*-type metal-organic frameworks

Baishu Zheng,[a] Zhen Yang,[b] Junfeng Bai,*[a] Yizhi Li[a] and Shuhua Li*[b]

[a]*State Key Laboratory of Coordination Chemistry, School of Chemistry and Chemical Engineering, Nanjing University, Nanjing 210093, China. E-mail:bjunfeng@nju.edu.cn; Tel: +86-25-83593384.*

[b]*Institute of Theoretical and Computational Chemistry, Nanjing University, Nanjing 210093, China. E-mail: shuhua@nju.edu.cn; Tel: +86-25-83686465.*

1. EXPERIMENTAL SECTION

1.1 Materials and General methods. All chemical reagents were obtained from commercial sources and, unless otherwise noted, were used as received without further purification. Elemental analyses (C, H, and N) were performed on a Perkin-Elmer 240 analyzer. The IR spectra were recorded in the 400-4000 cm^{-1} on a VECTOR TM 22 spectrometer using KBr pellets. 1H NMR spectra were recorded on a Bruker DRX-500 spectrometer with tetramethylsilane as an internal reference. Powder X-ray diffraction (PXRD) data were collected on a Bruker D8 ADVANCE X-ray diffractometer with Cu Kα radiation. Using a Philip X' Pert Pro system, variable temperature PXRD (VTPXRD) measurements were recorded after the sample had stayed at the respective temperature for 30 min in N_2 atmosphere.

1.2 Preparation of Linkers, H_6BTB and H_6TATB. Into a flask flushed with N_2, 1,3,5-benzenetribenzoic acid, H_3BTB[1], (1.3 g, 3.3 mmol) was placed and 60 mL of anhydrous THF was added. Oxalyl chloride (60 mL, 70 mmol) was slowly added dropwise with a syringe pump. The mixture was refluxed for 10 h and then the excess oxalyl chloride was removed under vacuum. To the resulting solid, 50 mL of anhydrous dimethylacetamide (DMA) was added and the solution was cooled with an ice bath. While under nitrogen flow, 4-(dimethylamino)pyridine (0.15 g, 1.2 mmol) was added followed by addition of 5-aminoisophthalic acid (2.2 g, 12.0 mmol). After stirring for 30 min at 0 °C and 48 hours at room temperature, the reaction solution was poured into a large excess of water. The precipitated solids were filtered off and washed repeatedly with hot methanol. The wet solid was finally dried in a vacuum oven at 100 °C to yield pure H_6BTB as a pale yellow powder (2.5 g, 81% yield). ^{1}H NMR (500MHz, DMSO-d_6, δ ppm): 13.308 (broad peak, 6H, COO$\underline{H}$), 10.711 (s, 3H, CON$\underline{H}$), 8.741 (s, 6H, Ar$\underline{H}$), 8.239 (s, 3H, Ar$\underline{H}$), 8.198 (s, 6H, Ar$\underline{H}$), 8.173 (s, 6H, Ar$\underline{H}$), 8.094 (s, 3H, Ar$\underline{H}$). Selected IR (KBr, cm^{-1}): 1702, 1601, 1542, 1454, 1427, 1330, 1282, 1233, 1109, 1010, 908, 836, 758, 661, 594. MP: > 300 °C. Replacement of H_3BTB with H_3TATB[2] under similar procedures afforded to **H_6TATB** in ~ 85% yield. Selected IR (KBr, cm^{-1}): 1705, 1604, 1551, 1516, 1450, 1406, 1364, 1330, 1280, 1245, 1104, 1015, 905, 873, 842, 820, 757, 663, 597. ^{1}H NMR (500 MHz, DMSO-d_6, δ ppm): 13.31 (broad peak, 6H, COO$\underline{H}$), 10.85 (s, 3H, CON$\underline{H}$), 8.96 (d, 6H, Ar$\underline{H}$), 8.74 (s, 6H, Ar$\underline{H}$), 8.31 (d, 6H, Ar$\underline{H}$), 8.26 (s, 3H, Ar$\underline{H}$). MP: > 300 °C.

1.3 Preparation of 1, $[Cu_3(BTB^{6-})]_n$. Linker H_6BTB (18.54 mg, 0.02 mmol) was added to a solution of *N*, *N*-dimethylformamide (DMF, 2 mL) with 0.3 mL concentrated HNO_3 in a 20-mL scintillation vial. To this mixture, $Cu(NO_3)_2 \cdot 3H_2O$ (25 mg, 0.1 mmol) was added, and the contents were sonicated until dissolved and then heated at 65 °C. After 72 hours, the mother liquor was decanted and replaced twice with fresh DMF. Pale blue polyhedral shape crystals were soaked in anhydrous acetone and then replaced with fresh acetone after every 8 hours in 3 days. Solvent was removed under vacuum for 4 hours and further dried at 100 °C for 20 hours to yield a deep purple-blue material (Fig. S2). The yield of the reaction based upon the weight of the solvent-free material is ~ 78 % based upon H_6BTB. Selected IR (KBr, cm^{-1}): 1666, 1549, 1380, 1279, 1097, 848, 770, 664. Anal. Calcd (Found) for $[Cu_3(C_{51}H_{27}N_3O_{15})]$: C, 55.06 (54.91) H, 2.45 (2.26) N, 3.78 (3.62).

1.4 Preparation of 2, $[Cu_3(TATB^{6-})]_n$. Linker H_6TATB (18.6 mg, 0.02 mmol) was added to a solution of 2 mL DMF/DMSO (1:1 in v/v) with 0.2 mL HBF_4 in a 20-mL scintillation vial.To this mixture, $Cu(NO_3)_2{\cdot}3H_2O$ (25 mg, 0.1 mmol) was added, and the contents were sonicated until dissolved and then heated at 75 °C. After 48 hours, the mother liquor was decanted and replaced twice with fresh DMF/DMSO. Pale blue polyhedral shape crystals were soaked in anhydrous acetone and then replaced with fresh acetone after every 8 hours in 3 days. Solvent was removed under vacuum for 4 hours and further dried at 100 °C for 20 hours to yield a deep purple-blue material. The yield of the reaction based upon the weight of the solvent-free material is ~ 82 % based upon H_6TATB. Selected IR (KBr, cm^{-1}): 1667, 1551, 1516, 1406, 1362, 1280, 1242, 1106, 1016, 826, 760, 720, 600. Anal. Calcd (Found) for $[Cu_3(C_{48}H_{24}N_6O_{15})]$: C, 51.69 (51.85) H, 2.17 (2.06) N, 7.53 (7.65).

The crystals of **1** and **2** are stable for common organic solvents (such as DMF, DMA, DMSO, methanol, ethanol, acetone, chloroform, CH_2Cl_2 and so on) except for water; they become opaque after exposure several minutes in air.

1.5 Crystal Structure Determination. Single crystal suitable for X-ray structure determination were selected and sealed in a capillary under a microscope. The X-ray diffraction intensity data were measured on a Bruker Smart Apex CCD diffractometer at room temperature using graphite monochromated Mo/Kα radiation (λ = 0.71073 Å). Data reduction was made with the Bruker Saint program. The structures were solved by direct methods and refined with full-matrix least squares technique using the SHELXTL package[3]. Non-hydrogen atoms were refined with anisotropic displacement parameters during the final cycles. Hydrogen atoms were placed in calculated positions with isotropic displacement parameters set to 1.2 × U_{eq} of the attached atom. The unit cell includes a large region of disordered solvent molecules, which could not be modeled as discrete atomic sites. We employed PLATON/SQUEEZE[4] to calculate the diffraction contribution of the solvent molecules and, thereby, to produce a set of solvent-free diffraction intensities; structures were then refined again using the data generated. In the structure, the benzene ring (C7-C8-C9-C10-C11-C12) moiety is disordered over two positions.

A summary of the crystallographic data is given in Table S3. CCDC 840576 contains the supplementary crystallographic data for **1**. The data can be obtained free of charge at www.ccdc.cam.ac.uk/conts/retrieving.html or from the Cambridge Crystallographic Data Centre, 12, Union Road, Cambridge CB2 1EZ, UK.

1.6 Low-Pressure Gas Sorption Measurements. The N_2 (99.999 %) and Ar (99.999 %) adsorption/desorption isotherms were measured volumetrically using a Micromeritics ASAP 2020 surface area and pore size analyzer up to saturated pressure at 77 K and 87 K, respectively. About 150 mg acetone-exchanged samples were charged into a sample tube and activated at 100 °C for 20 hours by using the “outgas” function of the surface area analyzer. The resulting mass of dried material was ~ 100 mg. Helium (99.999 %) was used for the estimation of the free space (dead volume), assuming that it is not adsorbed at any of the studied temperatures. To provide the relative pressure P/P_0 accurately at each data point, the saturation pressure P_0 was monitored and measured throughout the gases analyses by a dedicated saturation pressure transducer. The specific surface areas were determined using the Brunauer-Emmett-Teller (BET) and the Langmuir equation from the N_2 sorption data. When applying the BET theory, we made sure that our analysis satisfies the two consistency criteria as detailed by Walton and co-workers[5]. For the Langmuir surface areas, data from the whole adsorption data were used. Pore size distribution (PSD) were calculated using the density functional theory (DFT) model for Ar adsorption based on a slit pore geometry as implemented in the Micromeritics ASAP2020 software package.

1.7 High-Pressure Gas Sorption Measurements. Gravimetric CO_2 (99.995 %), CH_4 (99.999 %) and N_2 (99.999 %) adsorption measurements were performed on an IGA-003 gravimetric adsorption instrument (Hiden-Isochema, UK) over the 0-20 bar range at 273 K and 298 K. Prior to sorption measurements, about 110 mg acetone-exchanged samples were loaded into the sample basket within the adsorption instrument and then degassed under high vacuum at 100 °C for 20 hours to obtain about 70 mg fully desolvated materials. At each pressure, the sample mass was monitored until equilibrium was reached (within 25 minutes). The total gases uptake of the sample were calculated according to the literatures.[6]

1.8 Heats of Adsorption A virial-type[7] expression comprising the temperature-independent parameters a_i and b_i was employed to calculate the enthalpies of adsorption for CO_2 (at 273 and 298 K) on **1** and **2**. In each case, the data were fitted using the equation:

$$\ln P = \ln N + 1/T \sum_{i=0}^{m} a_i N^i + \sum_{j=0}^{n} b_j N^j$$

Here, P is the pressure expressed in Torr, N is the amount adsorbed in mmol/g, T is the temperature in K, a_i and b_j are virial coefficients, and m, n represent the number of coefficients required to adequately describe the isotherms (m and n were gradually increased until the contribution of extra added a and b

coefficients was deemed to be statistically insignificant towards the overall fit, and the average value of the squared deviations from the experimental values was minimized). The values of the virial coefficients a_0 through a_m were then used to calculate the isosteric heat of adsorption using the following expression.

$$Q_{st} = -R\sum_{i=0}^{m} a_i N^i$$

Q_{st} is the coverage-dependent isosteric heat of adsorption and R is the universal gas constant. The heat of CO_2 sorption for **1** and **2** in this manuscript is determined by using the excess sorption data measured in the pressure range from 0-20 bar (273 and 298 K), which is fitted by the virial-equation very well (R^2>0.9999, see Fig. S8).

2. COMPUTATIONAL DETAILS

2.1 GCMC Simulations. To evaluate the adsorption mechanism of CO_2 molecules in frameworks at a molecular level, Grand Canonical Monte Carlo (GCMC) simulations were performed to obtain the density distribution of CO_2 molecules within framework **1** at 1 bar and 273 K. The interactions between the framework of the MOF structure and CO_2 molecules are described via the Coulomb and Lennard-Jones (LJ) interactions. A rigid three-site EPM2 model of CO_2 molecule[8] was used to accurately reproduce the experimental critical point and liquid–vapor coexistence curve of CO_2 molecules. For the MOF **1**, all LJ parameters (Table S4) were taken from the Universal force field (UFF)[9] except for the Cu atom[10], while the corresponding partial charges are obtained by performing first-principles calculations on some small cluster models. As shown in Fig. S10, the partial charges obtained from first-principles calculations were only adopted in the green frame of each cluster model. To determine the ground-state spins of each cluster model, single-point energy calculations at the unrestricted B3LYP/6-31g** level were performed at different spin states. Then, the atomic charges are chosen from the lowest-energy spin with the Merz-Singh-Kollman (MK) scheme[11], where atomic charges are fitted to reproduce the electrostatic potential at number of points. To keep the neutral feature of MOF, the positive and negative charges are scaled slightly (< 5%). With this strategy, the obtained partial atomic charges for all atomic types in MOF material **1** are given in the Table S5. In addition, it should be noted that the mixing LJ parameters between different atomic types were calculated by the Lorentz-Berthelot mixing rule.

To eliminate the complexity in the simulations, framework **1** was treated as a “rigid” lattice and the atom positions for the activated state were obtained from the experimentally determined crystal structure by careful eliminating the disordered parts through the Diamond and Material Studio tools.

The simulation box consisted of one unit cell (a = b = c = 52.557 Å and $\alpha = \beta = \gamma = 90$ degrees) and contained more than 3000 atoms. Prior to GCMC simulations, the corresponding chemical potentials of bulk CO_2 were determined by the test-particle method proposed by Widom[12], where the configuration spaces were obtained from NPT molecular dynamics (MD) simulations at 1 bar and 273 K. At the thermodynamic adsorption equilibrium, the chemical potentials of the adsorbate in the adsorbed and bulk phases are equivalent. Therefore, GCMC simulations were carried out for the adsorption of CO_2 in MOF with input of above chemical potentials at 1 bar and 273 K. Four basic types of trial moves with equal probabilities were included in the simulation: translation, rotation, insertion, and deletion. The acceptance rate in the translation and rotation steps were controlled about 50 % by adjusting the maximum magnitudes of translation and rotation, respectively. For increasing the acceptance efficiency of insertion, the configuration-biased method[13] was used for the insertion step. The cutoff distance for the LJ interaction was 14.0 Å and the electrostatic interactions were calculated using the Particle Mesh Ewald method[14] with a real-space cutoff of 14.0 Å and a tolerance of 10^{-5}. Each GCMC simulation was totally run for 4×10^6 trial steps. The first 1×10^6 steps were used for the equilibration and the subsequent 3×10^6 steps were used for ensemble averages.

2.2 First-principles Calculation. To further analyze the binding energies between the MOF and CO_2 molecule at different adsorption sites, a series of First-principles calculations were performed for the complex of CO_2 molecule and several cluster models extracted from the MOF which represent different adsorption sites. All geometry optimizations were performed at the B3LYP/6-31G** level. Based on the optimized geometries, the binding energy were calculated with the correction of basis set superposition error (BSSE) at the B3LYP/6-311++G** level. All First-principles calculations in this work were performed with the Gaussian 03 program. The binding energy is expressed as $E_{\text{binding}} = E(CO_2/\text{cluster}) - E(\text{cluster}) - E(CO_2) + E_{\text{BSSE}}$.

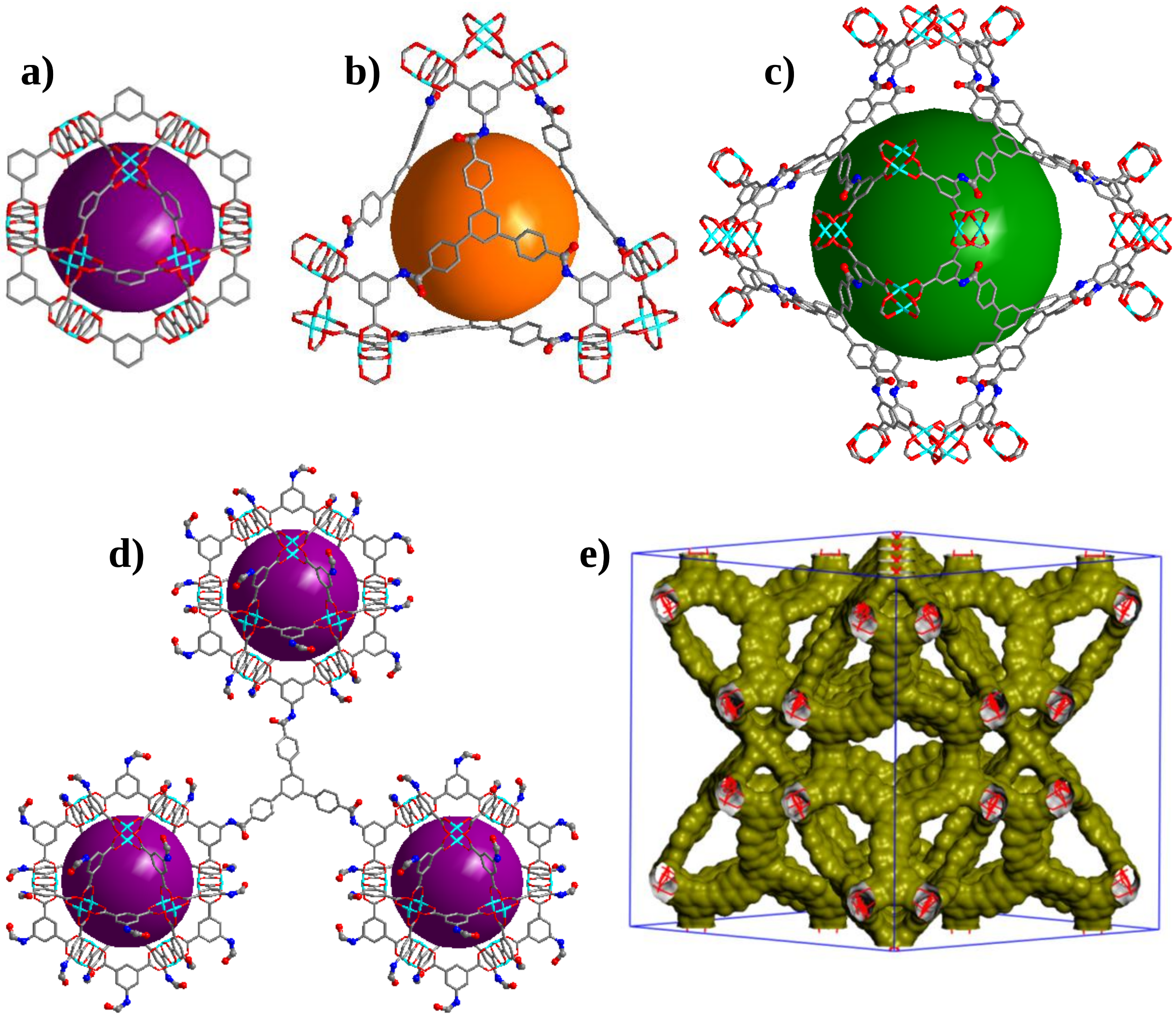

Fig. S1. Single-crystal structure of **1**. a-c) Three types of polyhedra (cub-Oh, T-Td and T-Oh). d) portion of structure of the (3, 24)-connected *rht*-type framework showing surface functionalization by acylamide groups. e) Solvent accessible surface area. Cu, blue-green; C, gray; O, red; N, blue. Water molecules and H atoms have been omitted for clarity.

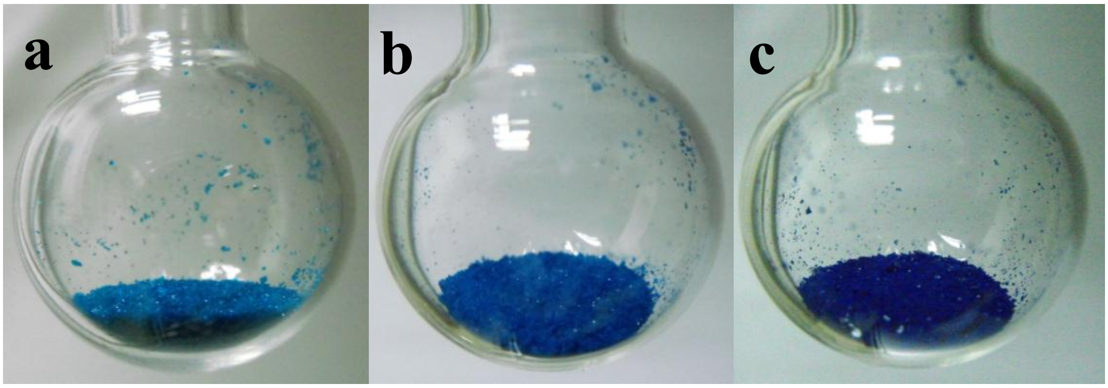

Fig. S2. Visual observation of color change in MOF materials **1** during activation (similar phenomenon was observed for **2**). Acetone-exchanged (a), after vacuum for 4 hours at room temperature (b), and then further activated at 100 ℃ for 20 hours (c).

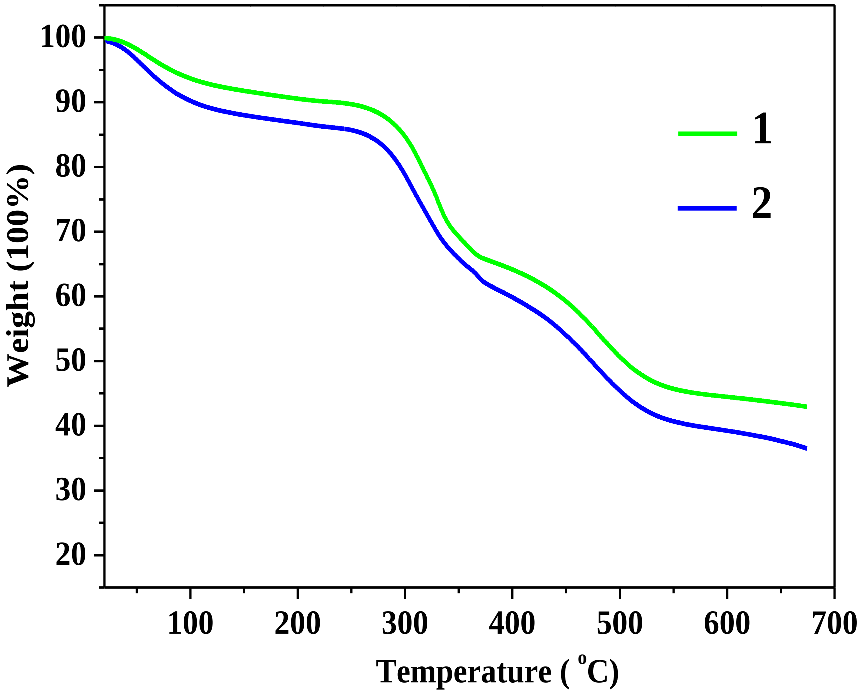

Fig. S3. TGA-curve for acetone-exchanged samples of **1** and **2**.

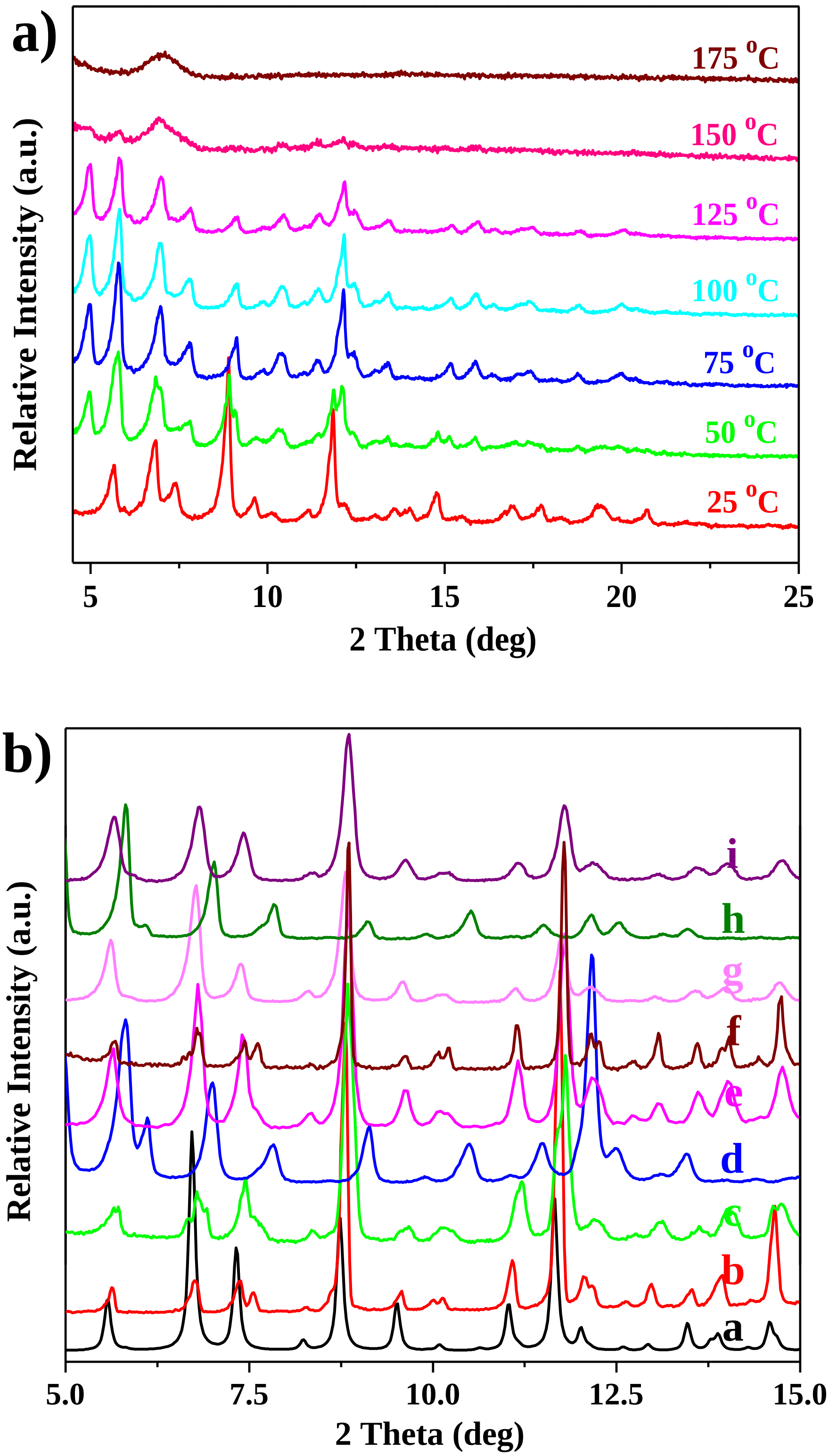

Fig. S4. The PXRD patterns. a) VPXRD patterns for **1**; b) a-e: simulated, as-synthesized, acetone-exchanged, activated, dried and then restored in anhydrous acetone for **1**; f-i: as-synthesized, acetone-exchanged, activated, dried and then restored in anhydrous acetone for **2**.

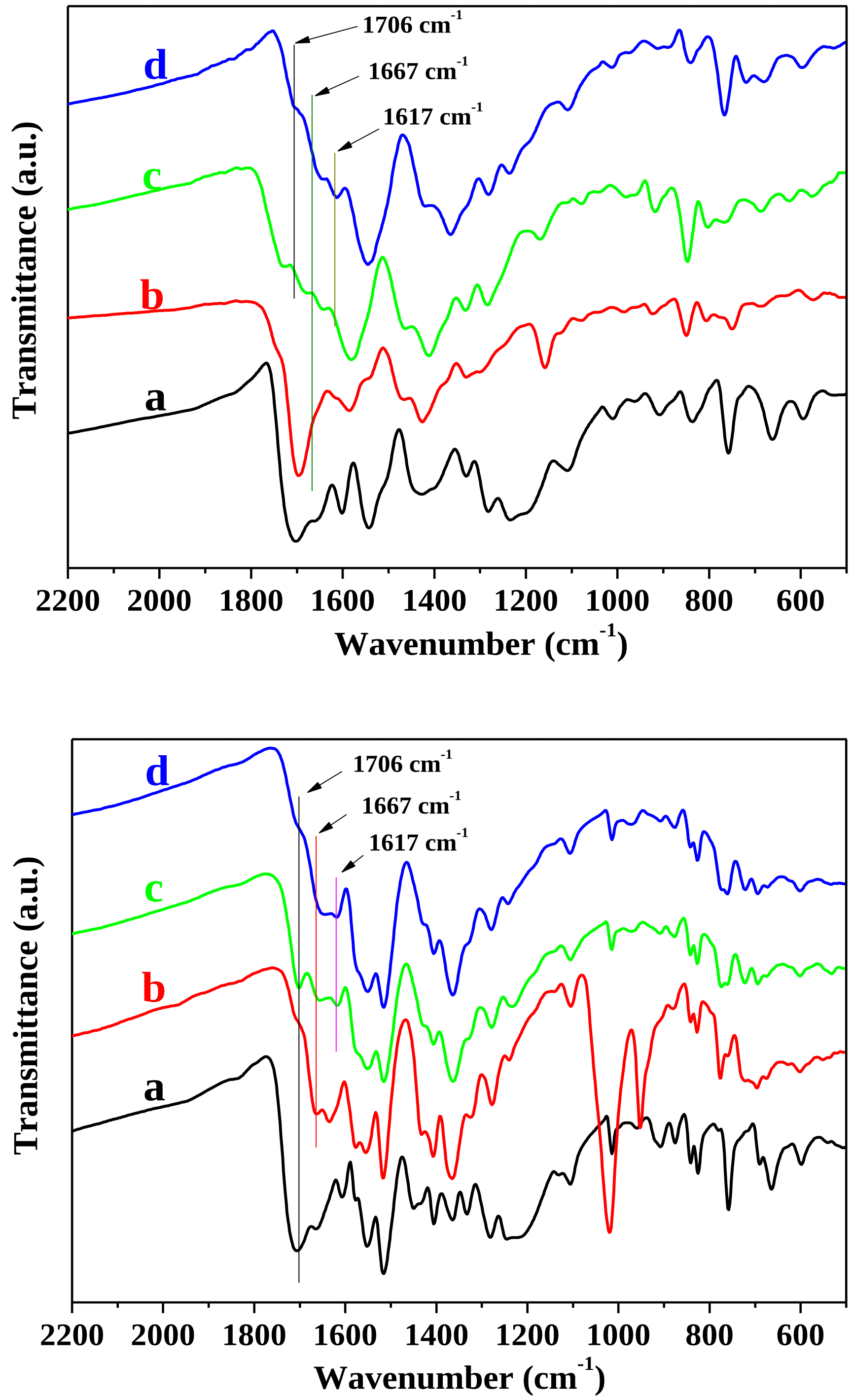

Fig. S5. The infrared spectra for **1** (top) and **2** (bottom). (a) ligand, (b) as-synthesized, (c) acetone-exchanged and (d) activated MOF materials. Note the absence of the vibration frequencies of the solvent DMF and acetone molecules in activated samples. The frequencies at 1667 cm^{-1} in (b) and 1706 cm^{-1} in (c) attribute to the *v* (CO) vibration of the DMF and acetone, respectively. The presence of the *v* (OH) stretching frequencies at 1617 cm^{-1} in both (c) and (d) may result from the rapid re-adsorption of trace moisture during the IR measurements.

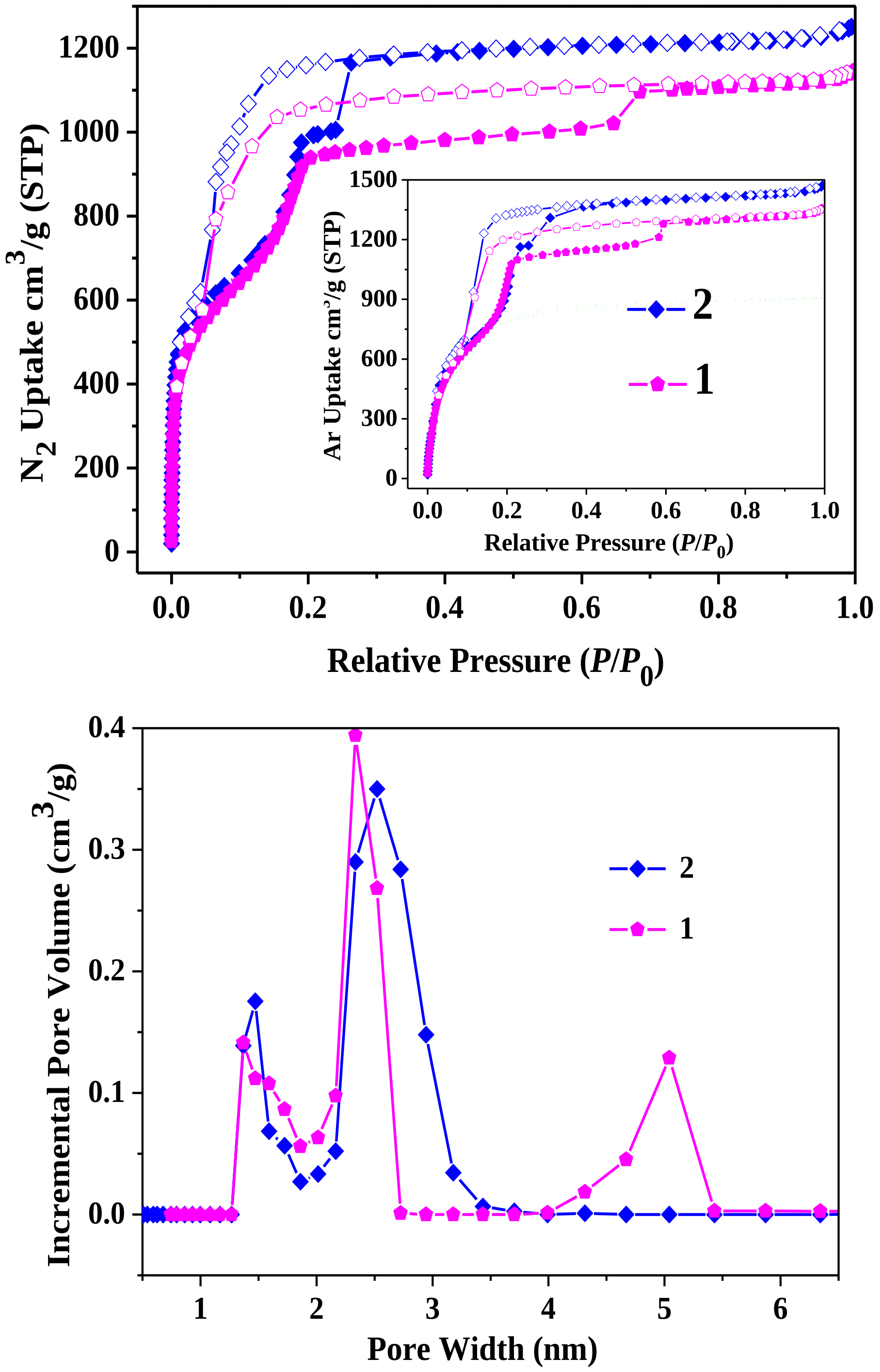

Fig. S6. Top: N_2 and Ar isotherms of MOF materials **1** and **2** collected at 77 and 87 K, respectively. Filled and open symbols represent adsorption and desorption, respectively. Bottom: Pore size distributions calculated from the Ar sorption isotherms based on DFT model in the Micromeritics ASAP2020 software package (assuming slit pore geometry).

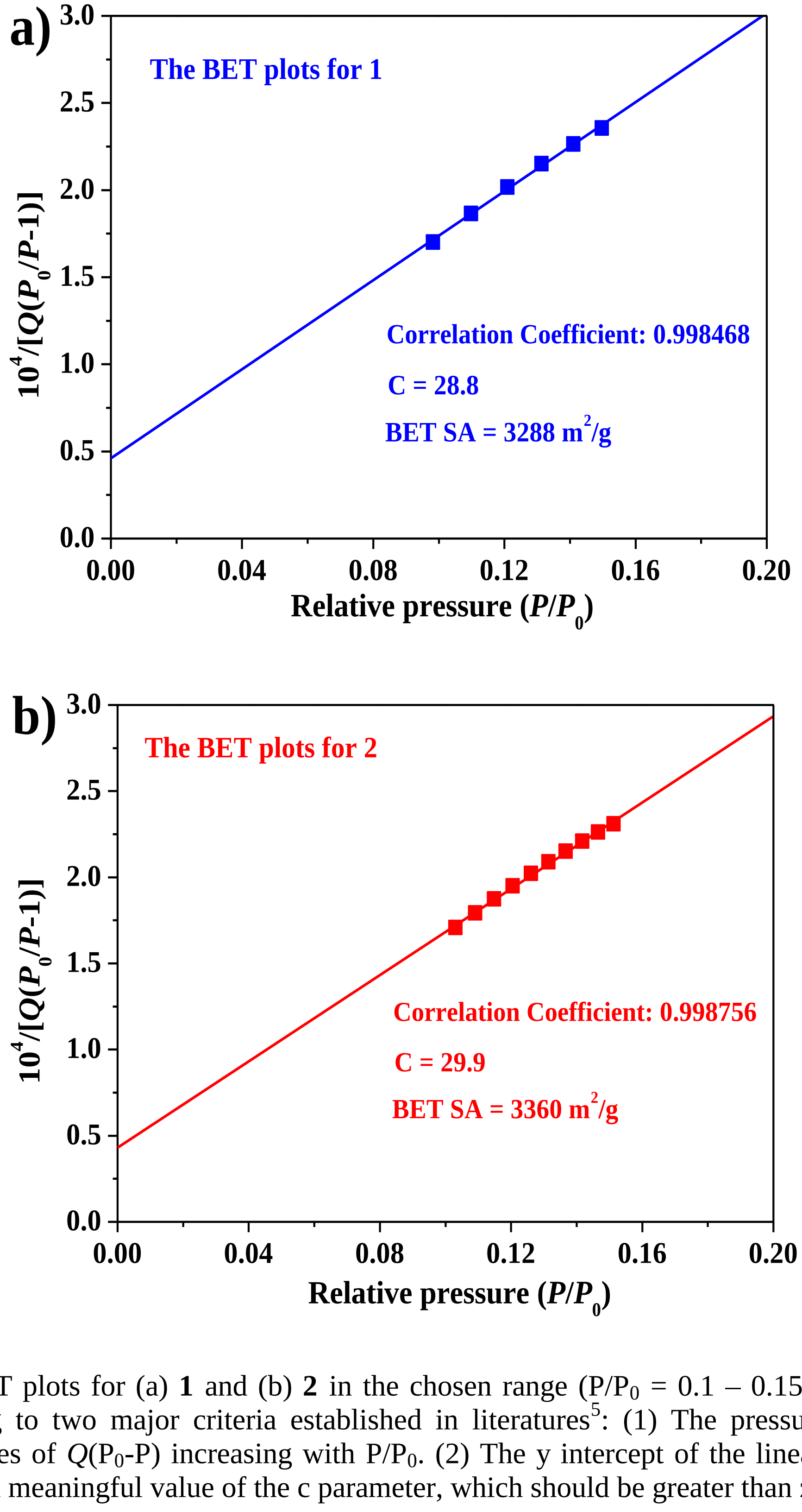

Fig. S7. The BET plots for (a) **1** and (b) **2** in the chosen range ($P/P_0 = 0.1 – 0.15$). This range was chosen according to two major criteria established in literatures[5]: (1) The pressure range selected should have values of $Q(P_0\text{-}P)$ increasing with P/P_0. (2) The y intercept of the linear region must be positive to yield a meaningful value of the c parameter, which should be greater than zero.

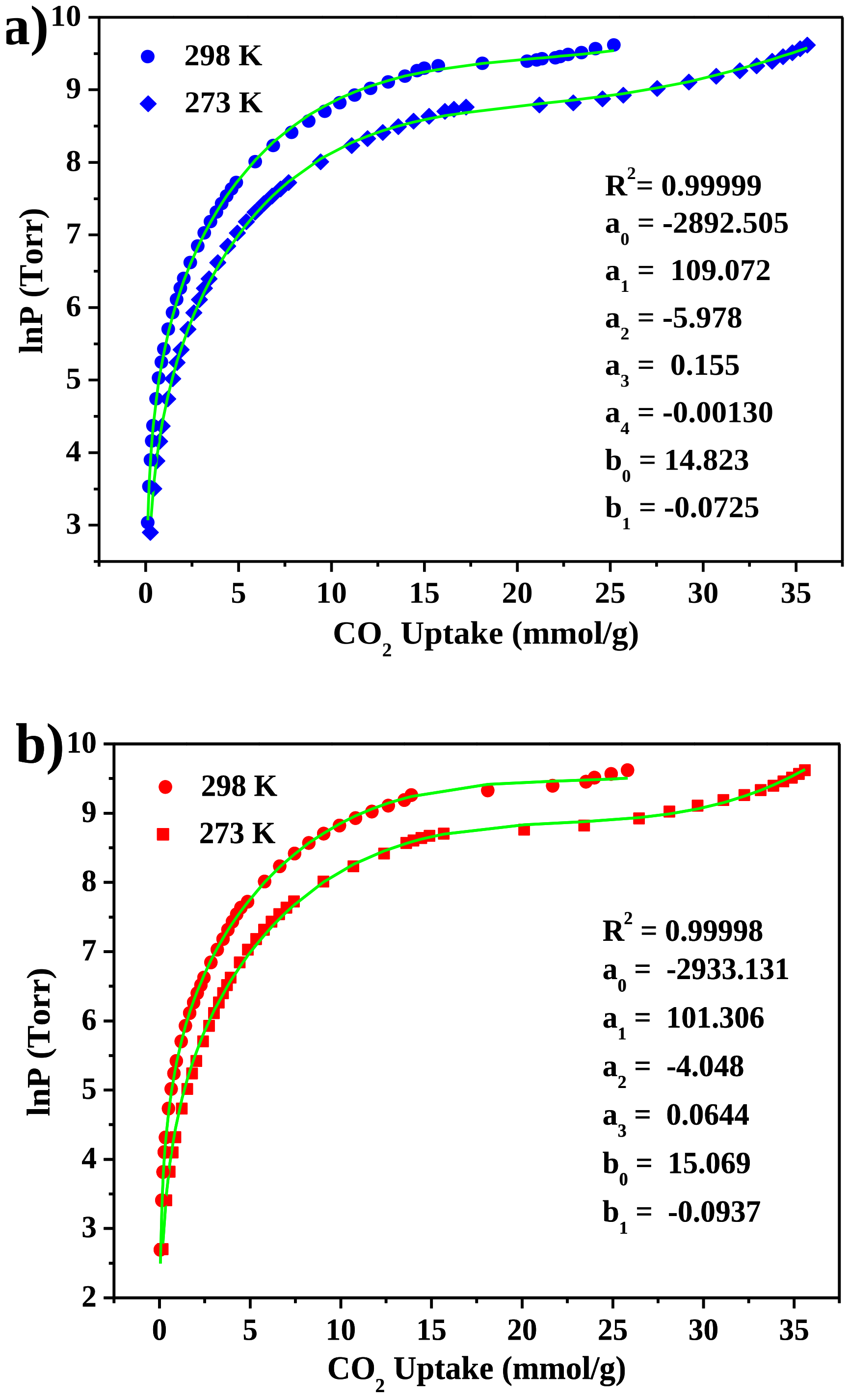

Fig. S8. Details of virial equation (solid lines) fitting to the experimental CO_2 adsorption data (symbols) for **1** a) and **2** b) collected at 273 and 298 K.

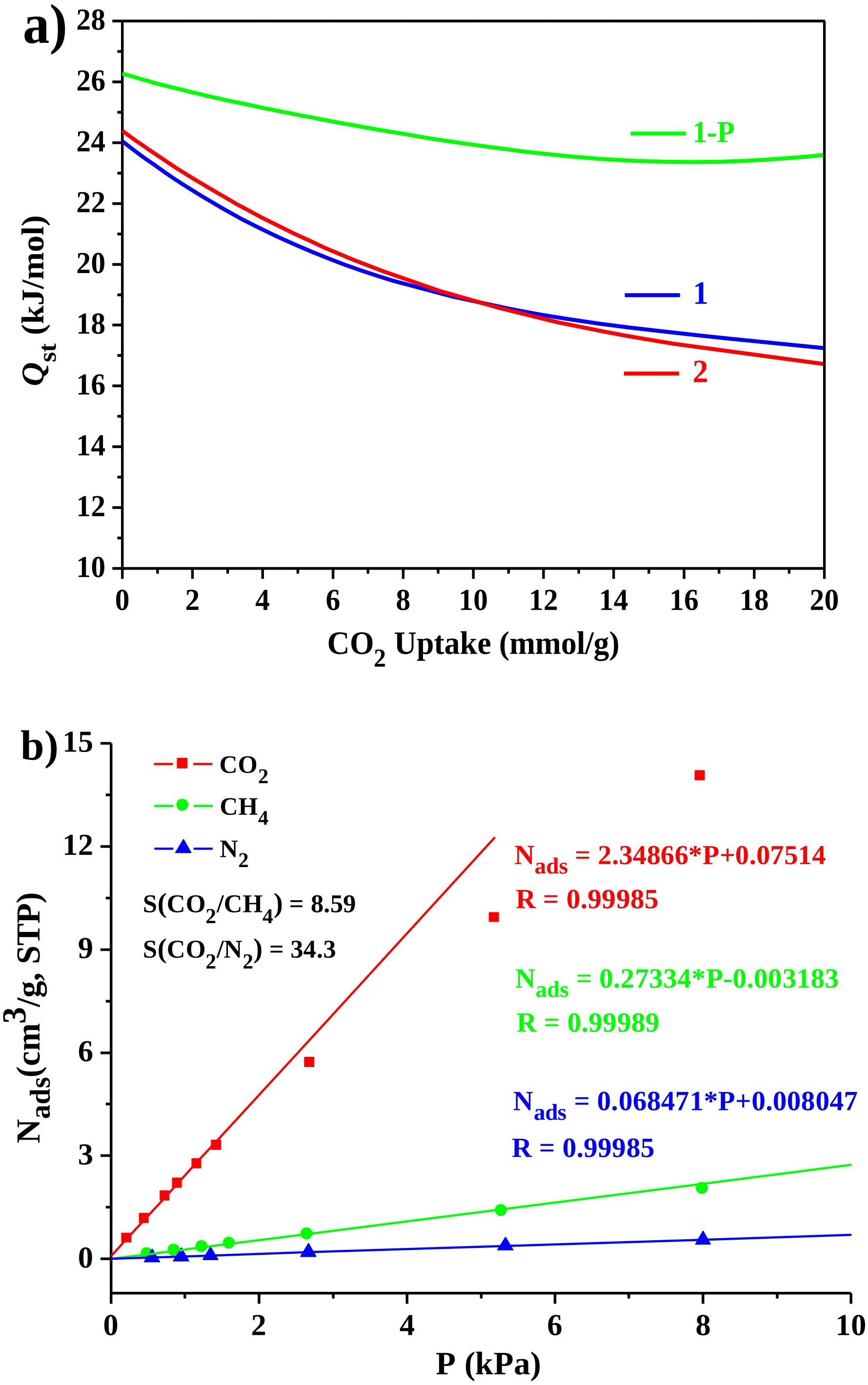

Fig. S9. a) The isosteric adsorption enthalpies for MOF materials **1**, **2** and **1-P**. b) The fitting initial slope for CO_2, CH_4 and N_2 isotherms for **1** collected at 273 K (N_{ads} = gases uptake; R = related coefficient). The calculated selectivity of CO_2/CH_4 and CO_2/N_2 for **1** is 8.6 and 34.3, respectively.

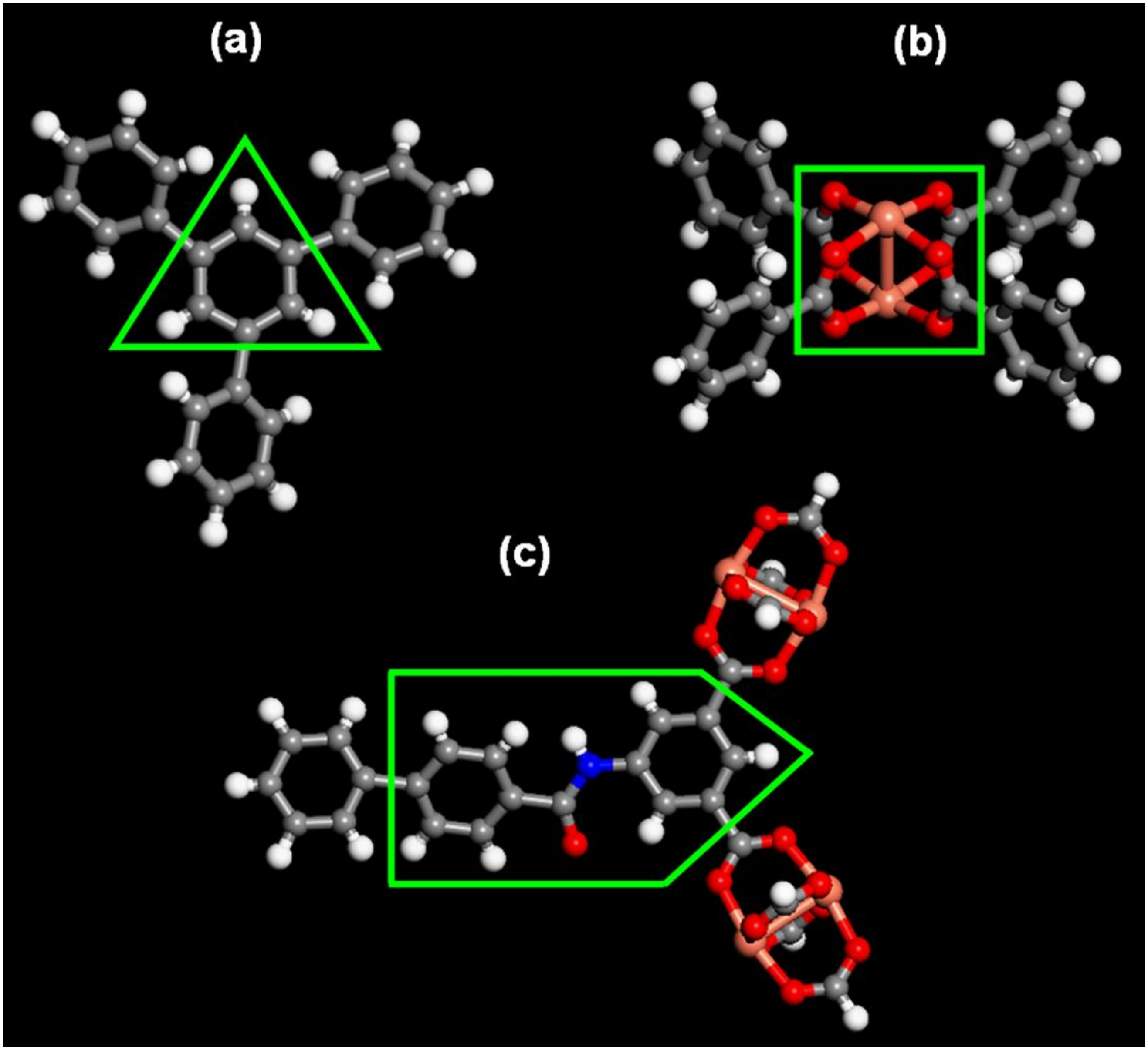

Fig. S10. Structural illustrations of three clusters used for deriving partial charges on atoms in framework **1**: (a) Cluster **A**, (b) Cluster **B**, and (c) Cluster **C**.

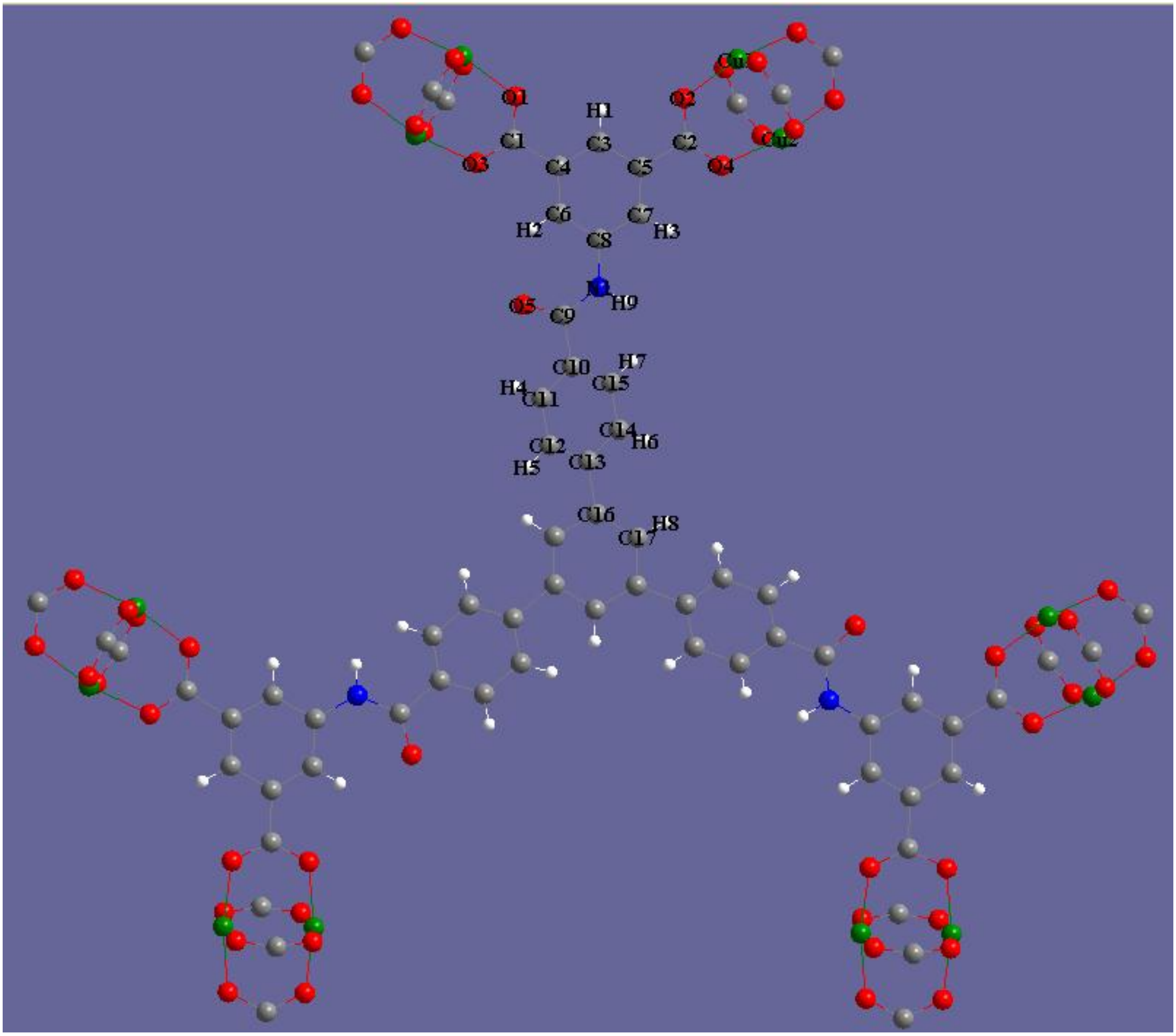

Fig. S11. The atomic schemes in framework of **1** used for GCMC and First-principles calculations.

Table S1. CO_2 sorption data for selected high surface area MOF materials

MOFs	**BET (m^2 g^{-1})**	**V_{Pore} (cm^3 g^{-1})**	**CO_2 Uptake (mmol g^{-1})^a**	**R_b**	**Q_{st} (kJ mol^{-1})**	**Ref**
MOF177	4750	1.89	28.0 (33.5)	14	15.7^c	15,16
MOF205	4460	2.16	26.0 (33.9)	12	NA^d	17
$Cu_3(BTB^{6-})$, **1**	3288	1.77	25.2 [35.6]	13	24.1	This work
$Cu_3(TATB^{6-})$, **2**	3360	1.91	25.2 [35.6]	13	24.4	This work
$Cu_3(TPBTM^{6-})$	3160	1.27	23.5 [27.6]	17	26.3	18
MIL-101	4230	2.15	22.5 (40.0)	12	44	15
PCN-69	3989	2.17	<22.5 (<35)	NA	NA	22
PCN-66	4000	1.63	22.1 (26.3)	12	26.2	19
PCN-68	5109	2.13	22.1 (30.4)	10	21.2	19
NU-100	6143	2.82	21.6 (46.4)	8	NA	20
PCN-61	3000	1.36	21.5 (23.5)	14	22.0	18,19
MOF-5	3800	1.55	19.0 (21.9)	13	15.9^c	16,21
MOF210	6240	3.60	16.0 (54.5)	5	NA^d	17
MOF200	4530	3.59	14.8 (54.4)	4	NA^d	17

[a] Excess value at 298 K and 20 bar, data in parentheses and square brackets represent saturated value reported at 298 K and unsaturated uptake at 20 bar (273 K). [b] Calculated times of absorbed CO_2 to empty-container. [c] Simulated value due to lack of experimental data. [d] NA, not available.

Table S2. CO_2 sorption data for some representative MOF (ZIF) materials with metal-free polar functional groups ($-NH_2$, -NH-, $-NO_2$, -OH, $-SO_3$-, -CONH-, etc)

MOF materials[a]	BET[b]	V_{pore}[c]	CO_2 sorption properties		Q_{st}[d]	ref
			Lower pressure	High pressure		
IMOF 3 [$-NH_2$]	802	0.34	2.14 mmol g^{-1}, 298 K, 1 bar	NA[e]	NA	23
IRMOF 3 [$-NH_2$]	2160	1.07	1.2 mmol g^{-1}, 298 K, 1.1 bar	18.7 mmol g^{-1}, 298 K, 35 bar	17.4	24
bio-MOF-11 [$-NH_2$]	1040	0.45	6.0 mmol g^{-1}, 273 K, 1 bar; 4.1 mmol g^{-1}, 298 K, 1 bar	NA	45	25
Amino-MIL-53(Al) [$-NH_2$]	NA	NA	NA	6.7 mmol g^{-1}, 303 K, 30 bar	38.4	26
$Zn_2(C_2O_4)(C_2N_4H_3)_2$ [$-NH_2$]	782	0.19	4.35 mmol g^{-1}, 273 K, 1.2 bar; 3.78 mmol g^{-1}, 298 K, 1.2 bar	NA	38.6	27
USO-1-Al-A [$-NH_2$]	960	0.25	3.2 mmol g^{-1}, 298 K, 1 bar	NA	50	28
rht-MOF-7 [-NH-]	(2170)	0.76	6.52 mmol g^{-1}, 273 K, 1 bar	NA	44.7	29
ZIF-78 [$-NO_2$]	620	NA	2.3 mmol g^{-1}, 273 K, 1.0 bar	NA	NA	30
$Cu_2(C_{40}H_{22}O_{10})$ [-OH]	(1217)	NA	2.9 mmol g^{-1}, 273 K, 1.0 bar	NA	NA	31
UoC-1 [$-SO_3$-]	(649)	0.24	2.0 mmol g^{-1}, 273 K, 1 bar	NA	NA	32
$Cu_3(BTB^{6-})$, **1** [-CONH-]	3288	1.77	3.90 mmol g^{-1}, 273 K, 1 bar; 2.45 mmol g^{-1}, 298 K, 1 bar	35.6 mmol g^{-1}, 273 K, 20 bar; 25.2 mmol g^{-1}, 298 K, 20 bar	24.1	This work
$Cu_3(TATB^{6-})$, **2** [-CONH-]	3360	1.91	3.94 mmol g^{-1}, 273 K, 1 bar; 2.47 mmol g^{-1}, 298 K, 1 bar	35.6 mmol g^{-1}, 273 K, 20 bar; 25.2 mmol g^{-1}, 298 K, 20 bar	24.4	This work

[a] Square brackets represent functional groups within the frameworks. [b] in m^2 g^{-1} and data in parentheses represent Langmiur surface area. [c] in cm^3 g^{-1}. [d] in kJ mol^{-1}. [e] NA, not available.

Table S3. Crystal data and structure refinement for **1**.

Identification code	**1**
CCDC number	840576
Empirical formula	C17 H11 Cu N O6
Formula weight	388.81
Temperature	291 (2) K
Wavelength	0.71073 Å
Crystal system	Cubic
Space group	Fm-3m
Unit cell dimensions.	$a = b = c = 52.557$ (3) Å, $\alpha = \beta = \gamma = 90^\circ$
Volume	145175 (13) $Å^3$
Z	96
Density (calculated)	0.427 g cm^3
Absorption coefficient	0.370 mm^{-1}
F(000)	18912
Crystal size	0.28 × 0.24 × 0.22 mm
Theta range for data collection.	1.55 to 26.00°
Limiting indices	$-64 <= h <= 64$, $-64 <= k <= 32$, $-63 <= l <= 64$
Reflections collected / unique	202502 / 6764 [R(int) = 0.0961]
Completeness	99.9 % (2theta = 52.00°)
Absorption correction	Semi-empirical from equivalents
Max. and min. transmission	0.9230 and 0.9035
Refinement method	Full-matrix least-squares on F^2
Data /restraints / parameters	6764 / 0 / 152
Goodness-of-fit on F^2	1.035
Final R indices [I>2sigma(I)]	R1 = 0.0398, wR2 ^{a} = 0.1094
R indices (all data)	R1 = 0.0620, wR2 ^{a} = 0.1202
Largest diff. peak and hole	0.168 and -0.387 e. $Å^{-3}$

^{a} $R1 = \Sigma\ ||F_o| - |F_c||/|F_o|$; $wR2 = [\Sigma\ w(\Sigma\ F_o^2 - F_c^2)^2/\Sigma\ w(F_o^2)^2]^{1/2}$.

Table S4. All LJ parameters for different atomic types in MOF material **1** used in GCMC simulations.

Atomic type	σ (Å)	ε (kcal/mol)
C (CO_2)	2.757	0.056
O (CO_2)	3.033	0.160
H (MOF)	2.646	0.044
C (MOF)	3.531	0.105
N (MOF)	3.356	0.069
O (MOF)	3.209	0.060
Cu (MOF)	1.841	0.043

Table S5. All partial atomic charges for the MOF material **1** used in GCMC simulations.

Atomic type	**Cu1**	**O2**	**O5**	**N1**	**C1**	**C2**
Charge (e)	1.114	-0.703	-0.516	-0.623	0.773	0.773
Atomic type	**C3**	**C4**	**C5**	**C6**	**C7**	**C8**
Charge (e)	-0.098	0.118	0.118	-0.213	-0.213	0.312
Atomic type	**C9**	**C10**	**C11**	**C12**	**C13**	**C14**
Charge (e)	0.627	-0.190	-0.069	-0.176	0.096	-0.176
Atomic type	**C15**	**C16**	**C17**	**H1**	**H2**	**H3**
Charge (e)	-0.069	0.006	-0.166	0.129	0.162	0.162
Atomic type	**H4**	**H5**	**H6**	**H7**	**H8**	**H9**
Charge (e)	0.111	0.127	0.127	0.111	0.121	0.334

References:

[1] a) D. Hu, and K. Ronald, *Org. Biomol. Chem.*, 2008, **6**, 151; b) S. Hong, M. Oh, M. Park, J. W. Yoon, J.-S. Chang and M. S. Lah, *Chem. Commun.*, 2009, 5397.

[2] Y. K. Park, S. B. Choi, H. Kim, K. Kim, B.-H. Won, K. Choi, J.-S. Choi, W.-S. Ahu, N. Won, S. Kim, D. H. Jung, S.-H. Choi, G.-H. Kim, S.-H. Cha, Y. H. Jhon, J. K. Yang and J. Kim, *Angew. Chem., Int. Ed.*, 2007, **46**, 8230.

[3] G. M. Sheldrick, *Acta Crystallogr. Sect. A*, 2008, **64**, 112.

[4] A. L. Spek, *J. Appl. Crystallogr.*, 2003, **36**, 7.

[5] a) K. S. Walton and R. Q. Snurr, *J. Am. Chem. Soc.*, 2007, **129**, 8552; b) J. Rouquerol, P. Llewellyn and F. Rouquerol, *Stud. Surf. Sci. Catal.*, 2007, **160**, 49.

[6] a) S. S. Kaye, A. Dailly, O. M. Yaghi, and J. R. Long, *J. Am. Chem. Soc.* 2007, **129**, 14176; b) H. Furukawa, M. A. Miller and O. M. Yaghi, *J. Mater. Chem.*, 2007, **17**, 3197.

[7] J. L. C. Rowsell and O. M. Yaghi, *J. Am. Chem. Soc.*, 2006, **128**, 1304.

[8] J. G.; Harris, K. H. Yung, *J. Phys. Chem.*, 1995, **99**, 12021.

[9] A. K. Rappe, C. J. Casewit, K. S. Colwell, W. A. Goddard III, W. M. Skiff, *J. Am. Chem. Soc.*, 1992, **114**, 10024.

[10] M. S. Santosh, A. P. Lyubartsev, A. A. Mirzoev, D. K. Bhat *J. Phys. Chem. B*, 2010, **114**, 16632.

[11] U. C. Singh, P. A. Kollman, *J. Comput. Chem.*, 1984, **5**, 129; b) B. H. Besler, K. M. Merz Jr, P. A. Kollman, *J. Comput. Chem.*, 1990, **11**, 431.

[12] B. Widom, *J. Chem. Phys.*, 1963, **39**, 2808.

[13] J. I. Siepmann, D. Frenkel, *Mol. Phys.*, 1992, **75**, 59.

[14] U. Essmann, L. Perera, M. L. Berkowitz, T. Darden, H. Lee, L. G. Pedersen, *J. Chem. Phys.*, 1995, **103**, 8577.

[15] R. Babarao, J. Jiang, *Langmuir*, 2008, **24**, 6270.

[16] A. Ö. Yazaydin, R. Q. Snurr, T.-H. Park, K. Koh, J. Liu, M. D. Levan, A. I. Benin, P. Jakubczak, M. Lanuza, D. B. Galloway, J. J. Low, R. R. Wills, *J. Am. Chem. Soc.*, 2009, **131**, 18198.

[17] H. Furukawa, N. Ko, Y. B. Go, N. Aratani, S. B. Choi, E. Choi, A. O. Yazaydin, R. Q. Snurr, M. O' Keeffe, J. Kim, O. M. Yaghi, *Science*, 2010, **329**, 424.

[18] B. Zheng, J. Bai, J. Duan, L. Wojtas, M. J. Zaworotko, *J. Am. Chem. Soc.*, 2011, **133**, 748.

[19] D. Q. Yuan, D. Zhao, D. F. Sun, H.-C. Zhou, *Angew. Chem., Int. Ed.*, 2010, **49**, 5357.

[20] O. K. Farha, A. ōzgür Yazayd, I. Eryazici, C. D. Malliakas, B. G. Hauser, M. G. Kanatzidis, S. T. Nguyen, R. Q. Snurr and J. T. Hupp, *Nat. Chem.*, 2010, **2**, 944.

[21] A. R. Millward, O. M. Yaghi, *J. Am. Chem. Soc.*, 2005, **127**, 17998.

[22] D. Yuan, D. Zhao and H.-C. Zhou, *Inorg. Chem.*, 2011, **50**, 10528.

[23] F. Debatin, A. Thomas, A. Kelling, N. Hedin, Z. Bacsik, I. Senkovska, S. Kaskel, M. Junginger, H. Müller, U. Schilde, C. Jäger, A. Friedrich, and H.-J. Holdt, *Angew. Chem., Int. Ed.* 2010, **49**, 1258.

[24] (a) Millward, A. R. and Yaghi, O. M. *J. Am. Chem. Soc.*, 2005, **127**, 17998-17999; (b) J. L. C. Rowsell, O. M. Yaghi, *J. Am. Chem. Soc.* 2006, **128**, 1304-1315.

[25] J. An, S. J. Geib and N. L. Rosi, *J. Am. Chem. Soc.* 2010, **132**, 38.

[26] S. Couck, J. F. M. Denayer, G. V. Baron, T. Remy, J. Gascon, F. Kapteijn, *J. Am. Chem. Soc.* 2009, **131**, 6326.

[27] R. Vaidhyanathan, S. S. Iremonger, K. W. Dawson and G. K. H. Shimizu, *Chem. Commun.* 2009, 5230.

[28] B. Arstad, H. Fjellvåg, K. O. Kongshaug, O. Swang, and R. Blom, *Adsorption* 2008, *14*, 755.

[29] R. Luebke, J. F. Eubank, A. J. Cairns, Y. Belmabkhout, L. Wojtas and M. Eddaoudi, *Chem. Commun.*, 2012, DOI: 10.1039/c1cc15962c.

[30] A. Phan, C. J. Doonan, F. J. Uribe-romo, C. B. Knobler, M. O'Keeffee and O. M. Yaghi, *Chem. Soc. Rev.* 2010, *43*, 58-67.

[31] S. Wu, L. Ma, L.-S. Long, L.-S. Zheng and W. Lin, *Inorg. Chem.*, 2009, **48**, 2436-2442.

[32] E. Neofotistou, C. D. Malliakas and P. N. Trikalitis, *Chem. Eur. J.* 2009, **15**, 4523-4527.